

EXPERIMENTAL AND NUMERICAL STUDY OF A HIGH-FLOWRATE, MULTI-CHANNEL PERMANENT MAGNET PUMP FOR SODIUM

L. Goldšteins^{1*}, *I. Buceniēks*¹, *L. Buligins*¹,
*N. Jēkabsons*¹, *K. Kravalis*¹, *O. Mikanovskis*^{1,2}

¹ *Institute of Physics, University of Latvia, 32 Miera str., Salaspils-1, LV-2169, Latvia*

² *Faculty of Civil and Mechanical Engineering, Mechanical Engineering and Mechanics, Riga
Technical University, 6B Kipsalas, Riga, LV-1048, Latvia*

* *e-Mail: Linards.Goldsteins@lu.lv*

This study investigates a high-flowrate, multi-channel electromagnetic permanent magnet pump (EMP) by comparing experimental and numerical results obtained using an electrical potential (inductionless) method. Experimental data, including pressure, flowrate, power, temperature, and magnet system rotation speed, were collected using EMP in the TESLA-EMP loop at the Institute of Physics, University of Latvia (IPUL) in Salaspils. A numerical calculation under the same conditions was performed using the COMSOL Multiphysics commercial software. A steady-state MHD calculation, employing the k - ε turbulence model while neglecting the induced magnetic field was performed. The results indicate qualitatively good agreement in the developed pressure under insulating inner wall conditions, suggesting a poor electrical contact between the sub-channels and a relatively low slip magnetic Reynolds number.

Introduction.

The technology of permanent magnet pumps (EMP) has been known for at least two decades [1]. In many cases, analytical methods can be applied to estimate the EMP performance, however, more complex designs require numerical methods [2]. Multi-channel designs pose particular challenges, as a single channel is divided into multiple sub-channels using reinforcement walls for mechanical integrity. The electrical conductivity of these dividing walls plays a crucial role for eddy current closure conditions. If the walls are electrically insulating and have poor electrical contact with liquid metal, eddy currents close within each sub-channel separately, leading to reduced pressure. This may necessitate higher EMP rotation speeds, which are limited by the available electrical motor power. In this paper, we investigate a large permanent magnet pump with three sub-channels operating with liquid sodium, using an experimental setup similar to that in [3], and employ a 3D numerical model for detailed analysis.

1. Numerical model of the multi-channel EMP.

1.1. Calculation of external magnetic field. To calculate induced currents using an inductionless approach, the external magnetic field in the gap between the outside ferromagnetic yoke and the magnets, where the channel with the liquid metal is located, must be known. This is determined through a separate calculation, as illustrated in Figs. 1*a,b*.

The boundary conditions include perfect magnetic conductors on the inner and outer radial surfaces and magnetic insulation at both axial boundaries (z -axis, Fig. 1*a*). The magnetization of the permanent magnets follows a Halbach array, assuming a remanent flux density $B_{\text{rem}} = 1.1$ T typical for $\text{Sm}_2\text{Co}_{17}$ magnets.

In Figs. 2*a,b*, the calculated magnetic field flux density is shown. The flux lines are essentially constant over the z -axis in (Fig. 2*a*) also; higher flux densities are found near

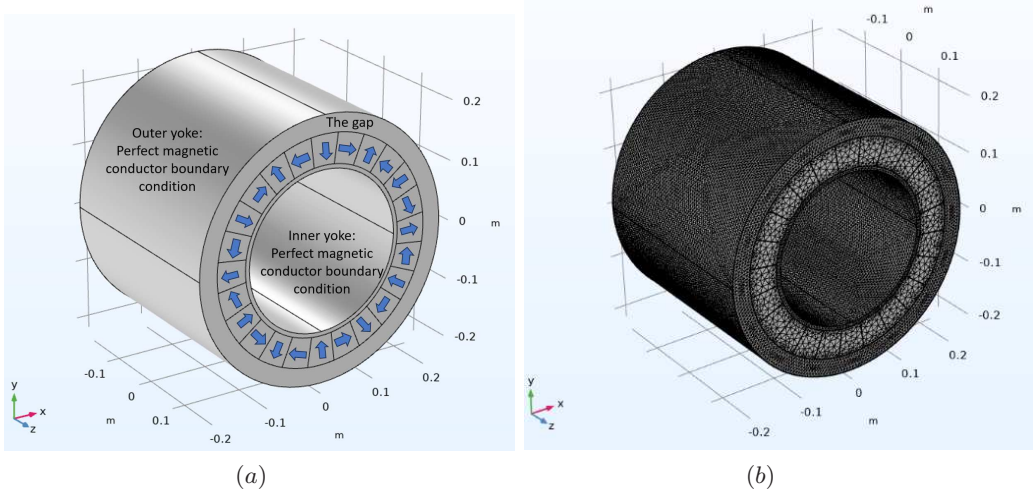


Fig. 1. (a) Geometry for magnetic field calculation. Arrows indicate the direction of magnetization. (b) Mesh used for magnetic field calculation. The mesh consists of 1 575 379 elements.

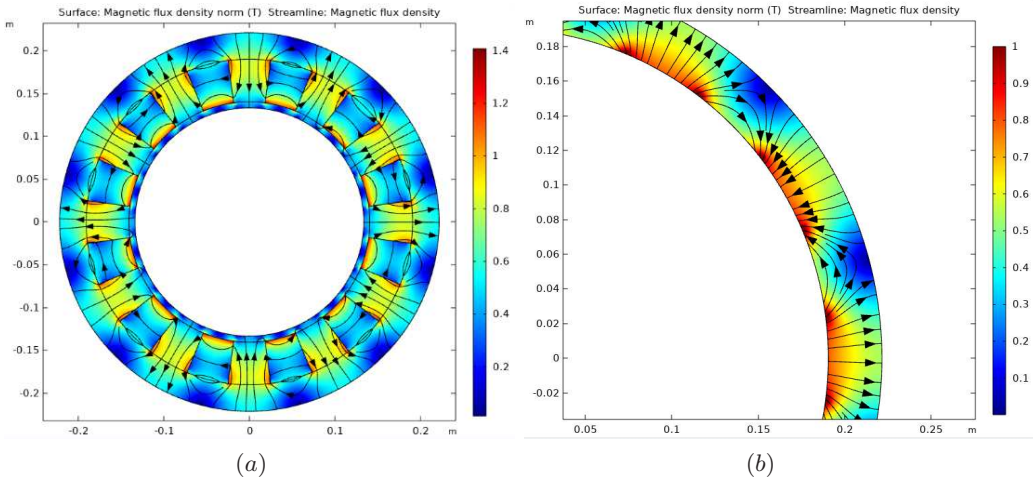


Fig. 2. (a) Calculated magnetic field in [T]. (b) Zoom of the magnetic field in the gap, location of the channel in [T].

the magnet corners. In Fig. 2b, a detailed view reveals that the field strength varies significantly in the gap over the radius reaching approximately 0.8 T near the inner wall and 0.4 T near the outside wall. This distribution is used for subsequent induced currents and MHD calculations.

1.2. *Calculations of induced currents and heat in empty channel walls.* This study estimates the proportion of the EMP motor power converted into channel heating. The channel made of stainless steel 316L is considered at a temperature of 200°C. Its respective geometry and the mesh used in calculations are shown in Figs. 3a,b. The electrical conductivity of the channel is $\sigma_w = 1.12 \text{ MS/m}$, the wall thickness is 3 mm (radial), 4 mm (side), 7 mm (middle), with the sub-channel height 20 mm and width 112 mm.

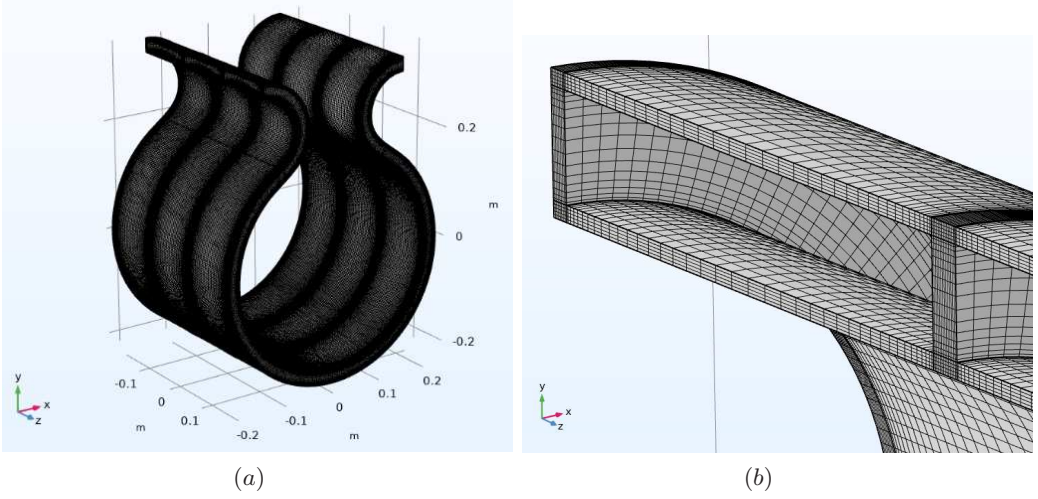


Fig. 3. (a) Geometry and mesh of the empty channel walls. The mesh consists of 1156900 elements. (b) Zoom of the mesh used for calculations. The cross-section of the channel walls is shown.

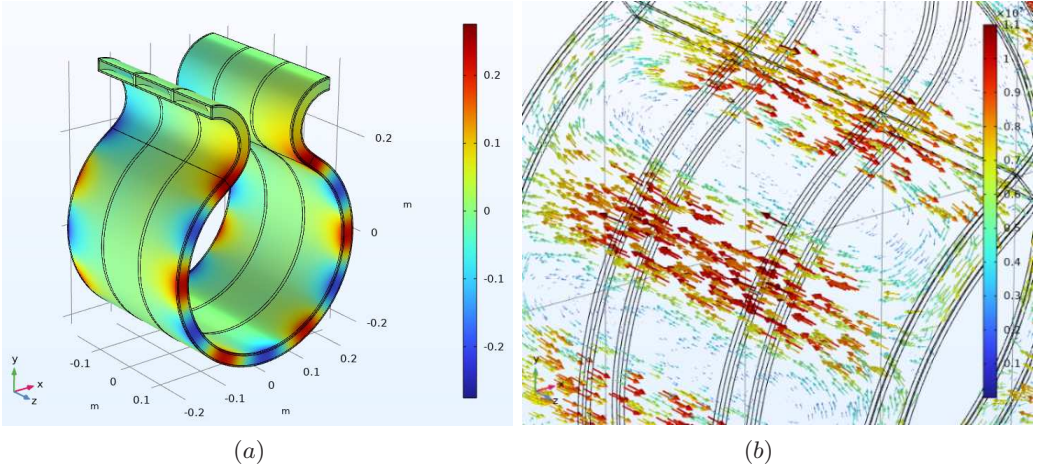


Fig. 4. (a) Distribution of the electrical potential in the empty channel walls in [V]. (b) Vectors of the eddy currents in the empty channel walls in [A/m²].

A stationary study was performed by solving the Poisson's equation (1) for the electrical potential φ , where the velocity \mathbf{v}_B of the magnetic field \mathbf{B} follows the solid body rotation Eq. (2), where r is the radial coordinate, n is the speed of the magnetic rotor, and θ is the angular coordinate. The electric current density \mathbf{j} was then computed using Eq. (3):

$$\Delta\varphi = \nabla \cdot (\mathbf{v}_B \times \mathbf{B}), \quad (1)$$

$$\mathbf{v}_B = 2\pi r \cdot n \cdot (\cos(\theta) \mathbf{e}_y - \sin(\theta) \mathbf{e}_x), \quad (2)$$

$$\mathbf{j} = \sigma_w (-\nabla\varphi + \mathbf{v}_B \times \mathbf{B}). \quad (3)$$

Insulating boundary conditions on the outside walls and zero potential at the inlet and outlet boundaries of the channel were applied. The rotation speeds $n = 4, 5.1, 6, 7.1, 8.1, 9.1, 10.1$ Hz were analyzed, and the results for $n = 10.1$ Hz are shown in Figs. 4a,b.

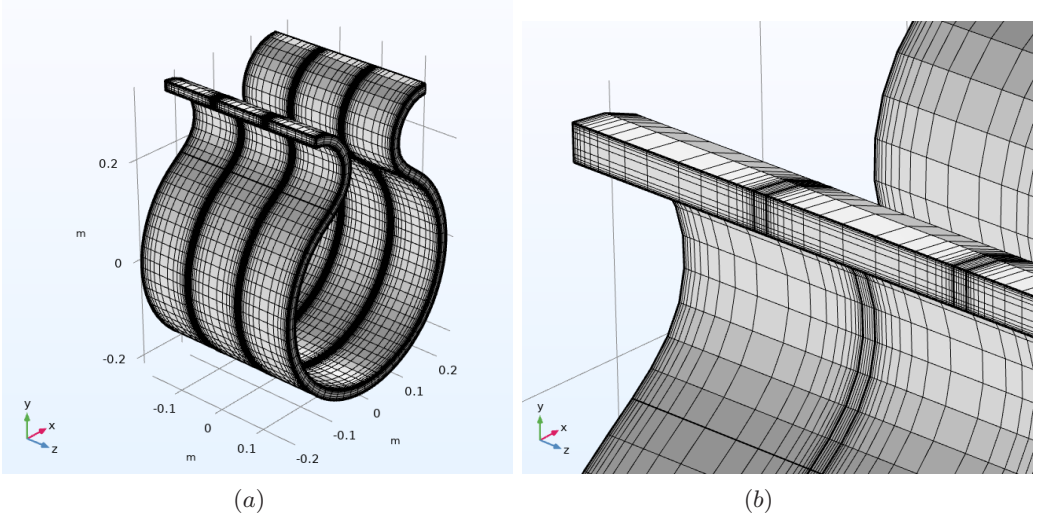


Fig. 5. (a) Geometry of the liquid metal layer and inner-walls. The mesh includes 84 315 elements. (b) Zoom of the mesh used for calculations. The cross-section of liquid metal and inner-walls is shown.

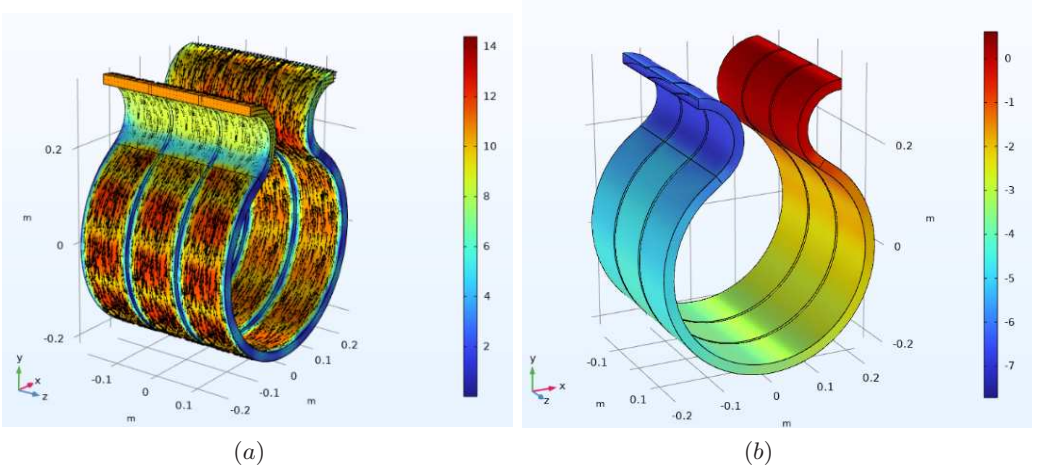


Fig. 6. (a) Velocity magnitude and vectors in [m/s]. $n = 10.1$ Hz, $Q = 76.6$ L/s. (b) Developed pressure in [bar]; $n = 10.1$ Hz, $Q = 76.6$ L/s.

1.3. MHD calculations in sub-channels. The flow of liquid sodium in the sub-channels divided by conducting or insulating walls was analyzed. The geometry and meshing details are shown in Figs. 5a,b.

The computational mesh comprises three sub-channels, each 20×112 mm with two 7-mm thick inner walls. The cross-section of each sub-channel is meshed with 15×21 elements, with a boundary layer thickness of $\delta = 0.054$ mm and a typical wall resolution of $y^+ \approx 50$, ensuring an adequate boundary layer resolution.

A stationary study was conducted by solving a coupled system of equations: the electrical potential equation (4), the Reynolds-Averaged Navier–Stokes (RANS) equation (5), and the continuity equation (6). The electromagnetic force term was added to Eq. (5),

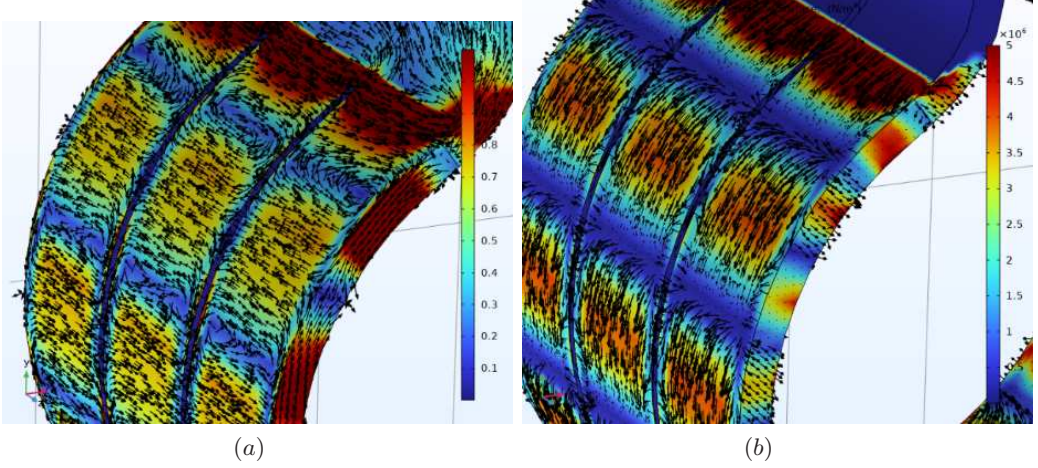


Fig. 7. (a) Eddy currents in $[A/m^2]$. $n = 10.1$ Hz, $Q = 76.6$ L/s. (b) Zoom of the EM force density in $[N/m^3]$; $n = 10.1$ Hz, $Q = 76.6$ L/s.

and the eddy viscosity μ_T was computed using the standard $k-\varepsilon$ model [4]. Electrical currents were calculated using Eq. (7):

$$\Delta\varphi = \nabla \cdot [(\mathbf{v}_B - \mathbf{v}) \times \mathbf{B}] \quad (4)$$

$$\rho(\mathbf{v}\nabla) \mathbf{v} = -\nabla p + (\mu + \mu_T) \Delta\mathbf{v} + \mathbf{j} \times \mathbf{B}, \quad (5)$$

$$\nabla \cdot \mathbf{v} = 0, \quad (6)$$

$$\mathbf{j} = \sigma(-\nabla\varphi + [(\mathbf{v}_B - \mathbf{v}) \times \mathbf{B}]). \quad (7)$$

The simulations considered a temperature of 200°C and the following sodium properties: $\sigma_{\text{Na}} = 7.78$ MS/m, $\rho_{\text{Na}} = 903.2$ kg/m³, $\mu_{\text{Na}} = 0.455$ mPa·s. A zero-pressure boundary condition was set at the outlet, with wall functions applied to the liquid boundaries.

The cases with the rotational speeds $n = 4, 5.1, 6, 7.1, 8.1, 9.1,$ and 10.1 Hz were analyzed based on the experimental data. For each rotational speed, the following flowrates were considered: $Q = 32.6, 40.5, 47.6, 55.4, 62.7, 70.3,$ and 76.6 L/s, as determined from the experiment. Corresponding to these flowrates, constant velocity inlet boundary conditions were applied (see Figs. 6,7).

The experimental data and that of the applied numerical models with insulating ($\sigma_w = 0$ S/m) or conducting walls ($\sigma_w = 1.12$ MS/m) are compared in Figs. 8,9. The total power was calculated using Eq. (8), where the final term on the right accounts for the power of both potential electromagnetic forces that contribute to pressure generation and vortical electromagnetic forces that stir the liquid metal but do not generate the EMP pressure:

$$P_{\text{Tot}} = P_w + P_{\text{Na}} + P_{\text{meh}} = \int \frac{j_w^2}{\sigma_w} dV_w + \int \frac{j_{\text{Na}}^2}{\sigma_{\text{Na}}} dV_{\text{Na}} + \int (\mathbf{v} \cdot \mathbf{f}) dV_{\text{Na}}. \quad (8)$$

The pumping power can be calculated as the product of the developed pressure and flowrate:

$$P_{\text{pump}} = \Delta p \cdot Q. \quad (9)$$

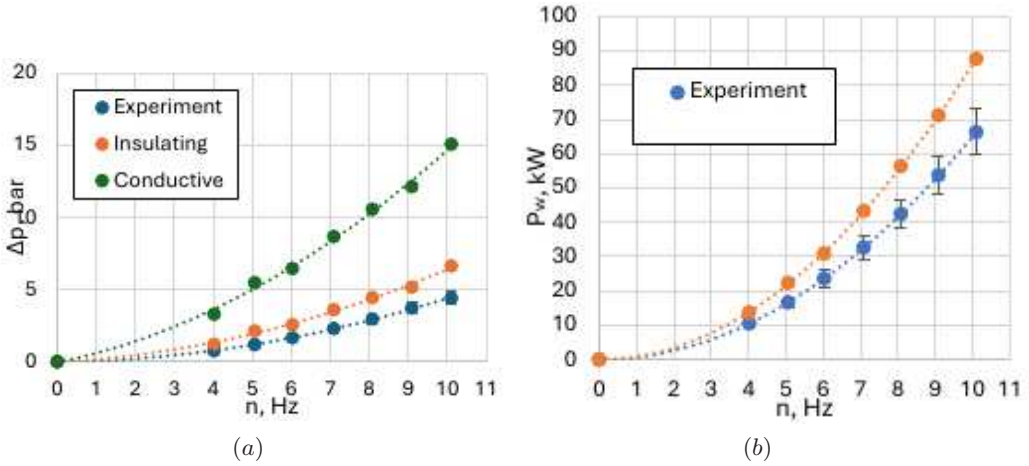


Fig. 8. (a) Comparison of the developed pressure. (b) Comparison of the heating power in the channel walls.

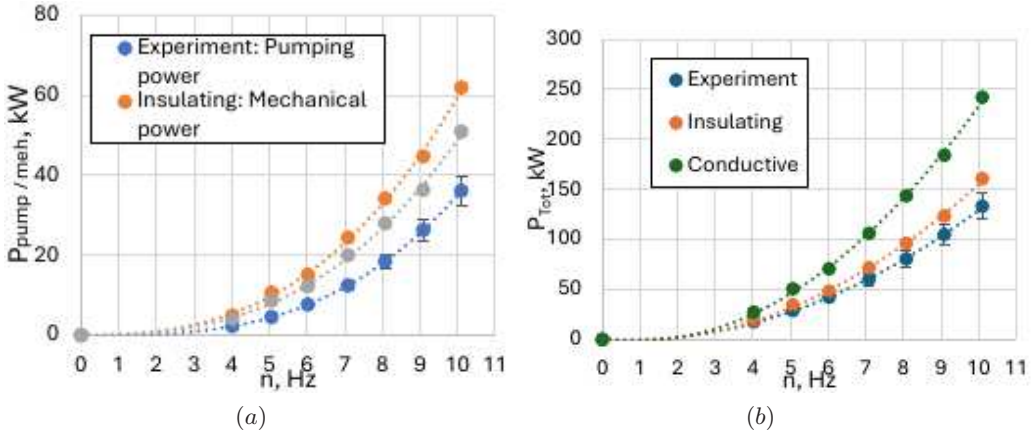


Fig. 9. (a) Comparison of pumping and mechanical power. (b) Comparison of the total power.

In Fig. 8a, a comparison of the developed pressure is presented. The results indicate that the conductivity of the inner walls has a significant impact as the developed pressure predicted by the model is increased by more than a factor of two when the conducting inner walls are considered. Although the experimental results for the developed pressure align more closely with the case of insulating inner walls, the model still overestimates the pressure difference.

In Fig. 8b, the generated heat in the channel walls is compared. A similar quadratic trend was observed in both the experimental and the numerical results, however, the model predicts higher Joule heating than what has been estimated experimentally [3].

In Fig. 9a, the experimentally measured pumping power Eq. (9) is compared with the modelled pumping and mechanical power. The results show that approximately 10 kW, or 17% of the mechanical power, is not converted into the pumping power. Additionally, the model overestimates the pumping power relative to the experiment, which is also evident in Fig. 8a.

Finally, when comparing the total power in Fig. 9a, much better agreement with the experimental data is observed for the insulating wall case. In contrast, the conducting wall case overestimates the total power by more than 100 kW, corresponding to an 82% deviation from the experimental results.

2. Conclusions and discussion.

A 3D model of a multi-channel EMP has been developed, capturing key MHD phenomena under the inductionless approximation. A reasonable agreement was obtained between the numerical results and the experimental data when assuming insulating inner walls (Figs. 8b, 9a), whereas the conducting inner wall model overestimates the EMP performance.

The results obtained suggest that the EMP inner walls behave as electrical insulators rather than conductors. Improving electrical contact would require the removal of oxide layers from the walls. However, in praxis, it is hard to do prior to experiments due to the channels complex geometry, and it was not performed. This limitation may partly explain the observed behavior of the EMP in the experiment.

The presented study (Figs. 8a, 9b) demonstrates that controlling the transversal current closure conditions in multi-channel EMP designs is crucial, as the design parameters such as the maximum pressure and the total power can vary by almost 100%. From the design prospect, this would imply the need to adjust factors such as the channel cross-section area, wall thickness for mechanical integrity, and the selection of a sufficiently powerful motor to ensure the achievement of the required working conditions.

Finally, the remaining discrepancies between the experiment and the numerical insulating wall cases may be attributed to the variations in remanent flux density of permanent magnets, which influences the developed pressure quadratically. The influence of transient and non-isothermal conditions in the channel, resulting from significant Joule heating, is not considered in this study. The local temperature in the channel and in the liquid metal may differ slightly from those measured in the loop, potentially affecting the electrical conductivity of the materials and, hence, the presented comparisons.

References

- [1] I. BUCENIEKS. *Magnetohydrodynamics*, vol. 39 (2003), no. 4, pp. 411–418.
- [2] L. GOLDŠTEINS, L. BULIGINS. *Magnetohydrodynamics*, vol. 48 (2012), no. 4, pp. 623–636.
- [3] A. BRĒKIS, L. BULIGINS, I. BUCENIEKS, L. GOLDŠTEINS, K. KRAVALIS, A. LĀCIS, O. MIKANOVSKIS, N. JĒKABSONS. *Fusion Engineering and Design*, vol. 194 (2023).
- [4] B.E. LAUNDER AND D.B. SPALDING. *Computer Methods in Applied Mechanics and Engineering*, vol. 3 (1974), no. 2, pp. 269–289.

Received 24.11.2024